Electronic Supplementary Material (ESI) for Dalton Transactions.

Supporting Information for:

Re-Silane Complexes as Frustrated Lewis Pairs for Catalytic Hydrosilylation

Caleb A. Brown, Michael Abrahamse and Elon A. Ison*

Department of Chemistry, North Carolina State University, 2620 Yarbrough Drive, Raleigh, North Carolina 27695-8204, United States

Table of Contents

ADDITIONAL KINETIC DATA

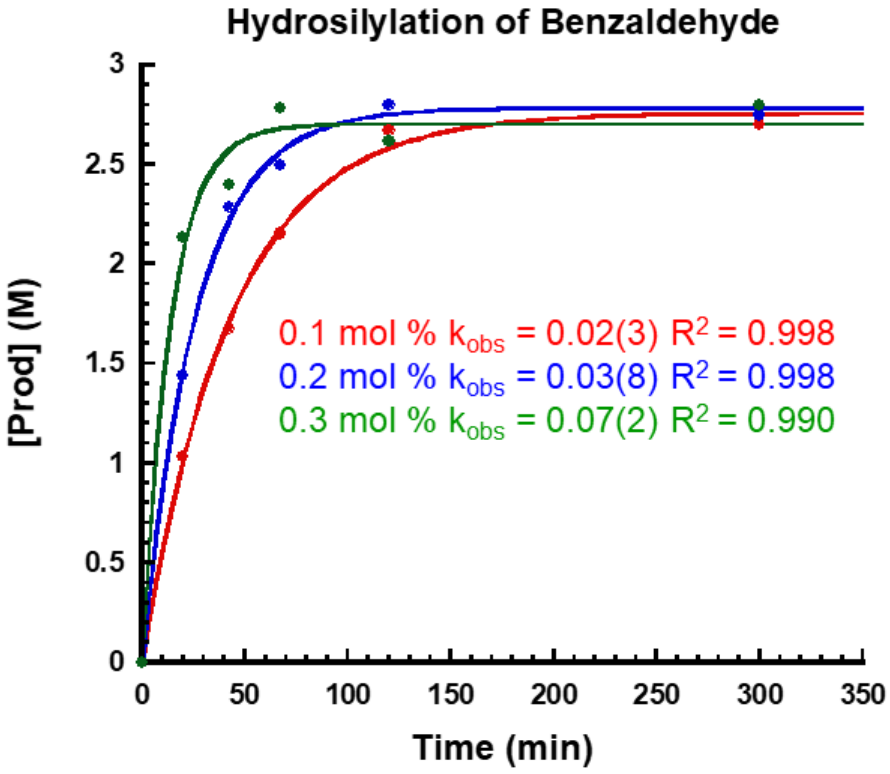

Figure S1. Time Profiles for Determination of Order with Respect to Re. 18 was dissolved in 0.25 mL (2.46 mmol) benzaldehyde, 0.38 mL (2.49 mmol) dimethylphenylsilane, and 0.34 mL (2.46 mmol) mesitylene. The reaction mixture was then divided into screw cap NMR tubes at run 80 °C. At each time point deuterated chloroform was added to the screw cap NMR tube and the product concentration was determined by ^{1}H NMR spectroscopy.

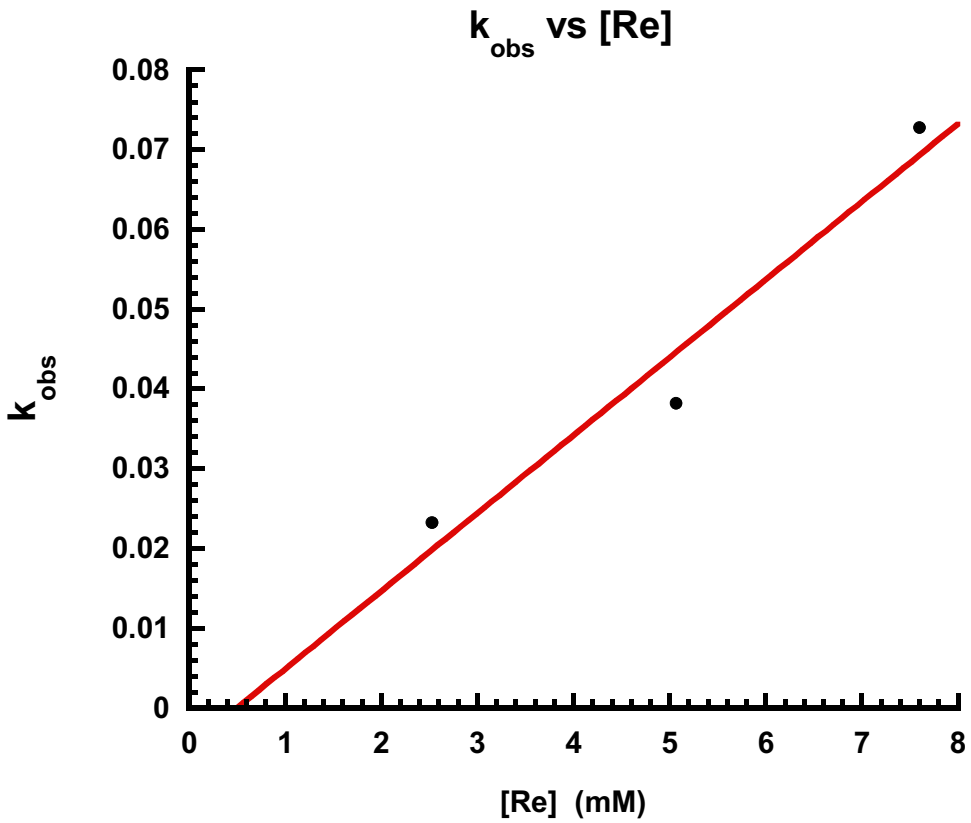

Figure S2. Plot of k_{obs} vs [Re]. The rhenium complex was dissolved in 0.25 mL (2.46 mmol) benzaldehyde, 0.38 mL (2.49 mmol) dimethylphenylsilane, and 0.34 mL (2.46 mmol) mesitylene. The reaction mixture was then divided into screw cap NMR tubes at run 80 °C. At each time point deuterated chloroform was added to the screw cap NMR tube and the product concentration was determined by ^{1}H NMR spectroscopy. The extracted k_{obs} was then plotted against concentration of **18**.

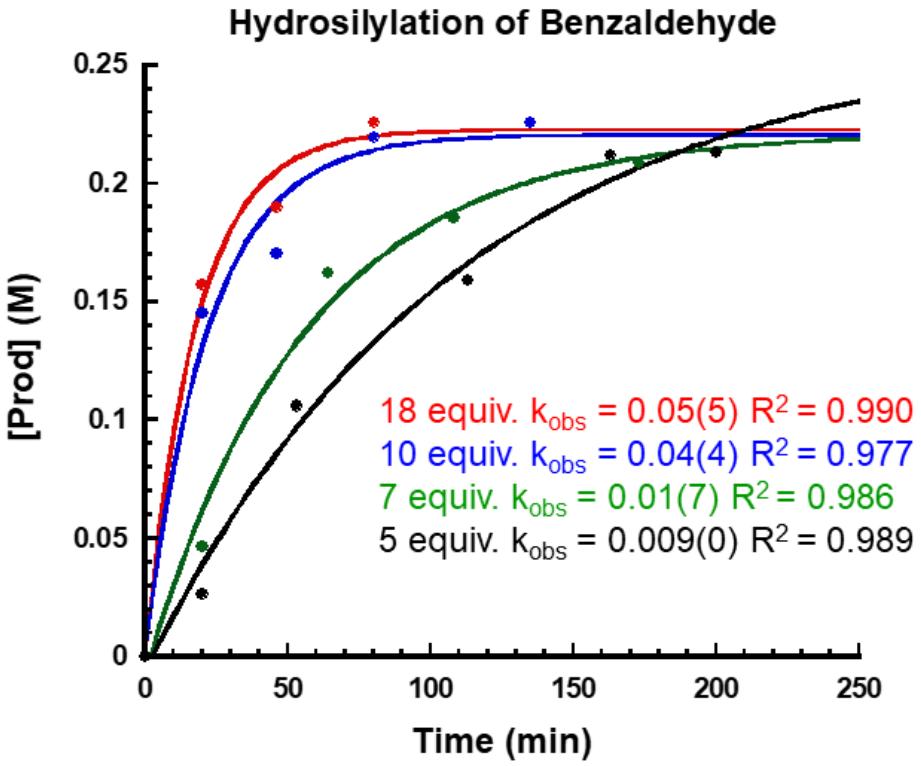

Figure S3. Time Profiles for Hydrosilylation in Excess Dimethylphenylsilane. The rhenium complex was dissolved in 0.125 mL (1.23 mmol) benzaldehyde and the appropriate equivalents of dimethylphenylsilane. The resulting solution was then diluted to a volume of 4.07 mL with the addition of mestilyene. The reaction mixture was then divided into 0.1 mL aliquots and placed into screw cap NMR tubes at run 80 °C. At each time point deuterated chloroform was added to the screw cap NMR tube and the product concentration was determined by ^{1}H NMR spectroscopy.

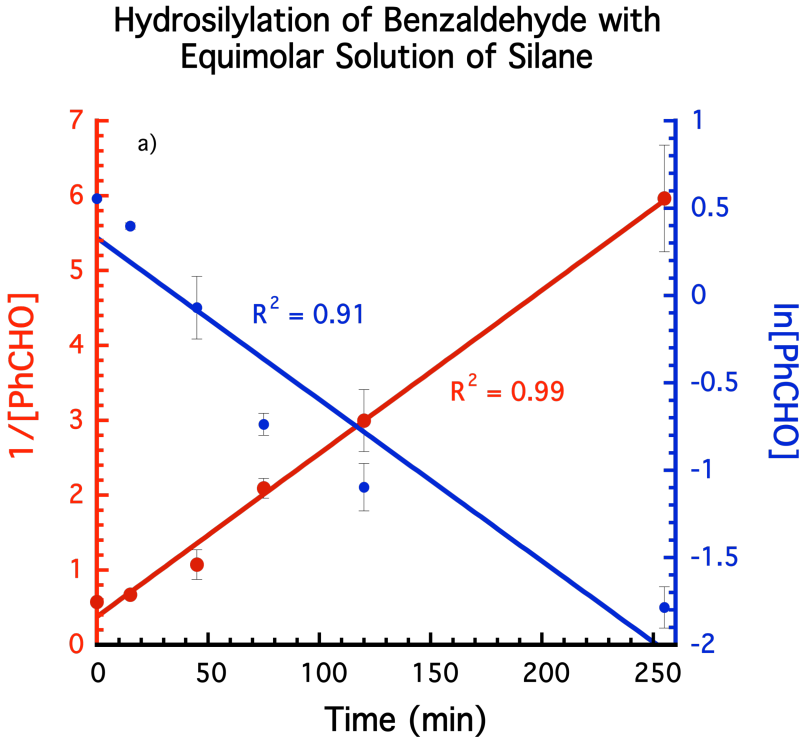

Figure S4. Kinetic plots for the catalytic hydrosilylation of benzaldehyde and dimethylphenylsilane at 80 °C with DAAmRe(CO)(OAc) (0.1 mol%). A) Data are fit to the integrated rate equation for a 1st order reaction (ln[PhCHO] (blue)) and a 2nd order reaction (1/[PhCHO] (red)). B) Linear fit of the observed rate constant versus the mol% of the rhenium catalyst.

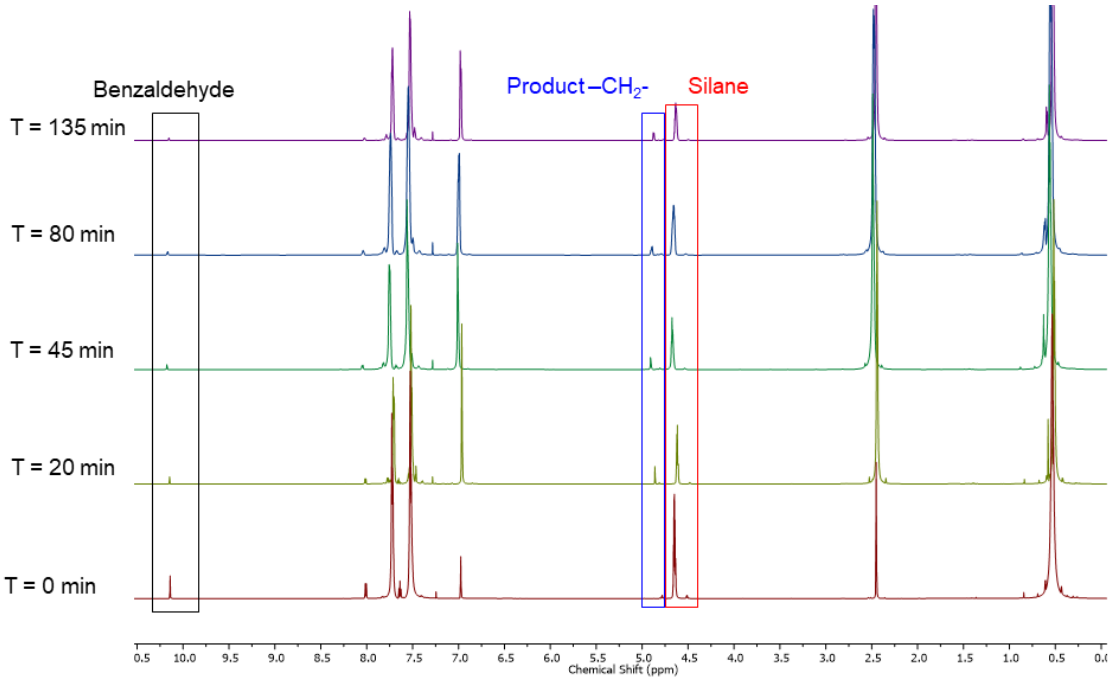

Figure S5. ^{1}H NMR Time Course of Catalytic Hydrosilylation of Benzaldehyde. The rhenium complex was dissolved in 0.125 mL (1.23 mmol) benzaldehyde and 2.83 mL (18.45 mmol) dimethylphenylsilane. The resulting solution was then diluted to a volume of 4.07 mL with the addition of mestilyene. The reaction mixture was then divided into 0.1 mL aliquots and placed into screw cap NMR tubes at run 80 °C. At each time point deuterated chloroform was added to the screw cap NMR tube and the product concentration was determined by ^{1}H NMR spectroscopy.

^{1}H NMR SPECTRA OF HYDROSILYLATION PRODUCTS

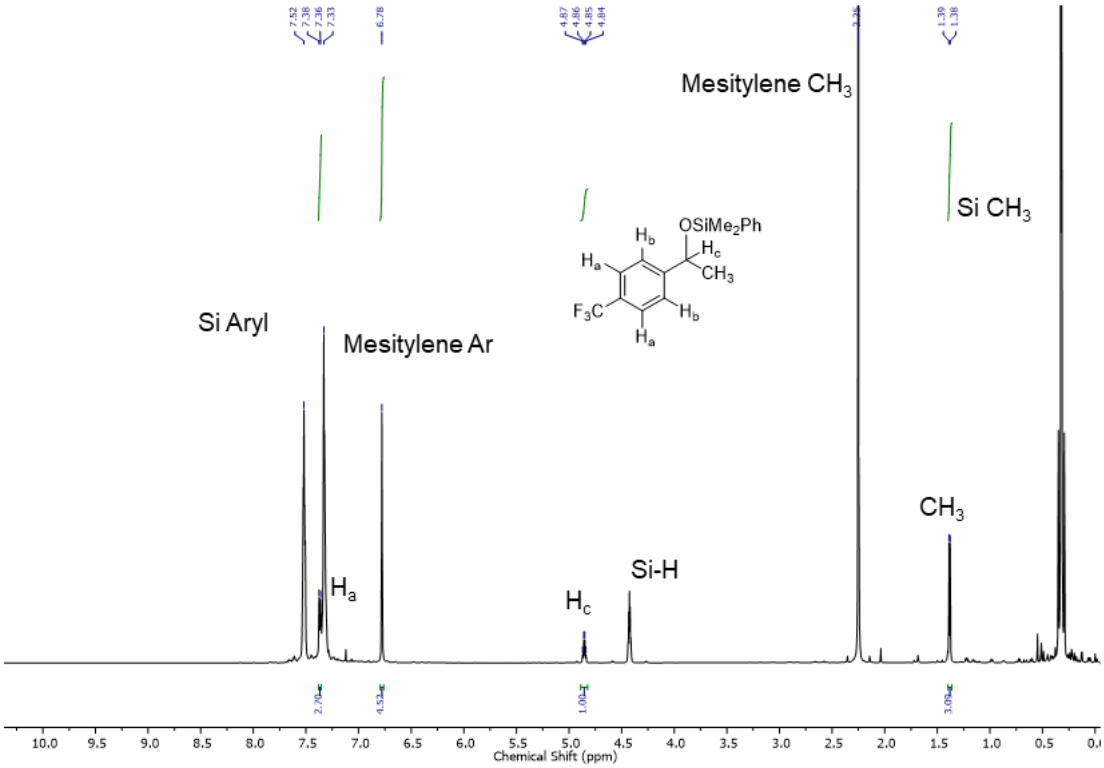

Figure S6. ^{1}H NMR Spectrum of dimethyl(phenyl)(1-(4-(trifluoromethyl)phenyl)ethoxy)silane. ^{1}H NMR (Chloroform-*d*, 600 MHz) δ: 7.37(d, *J* = 8.1 Hz, 2H), 4.86 (q, *J* = 6.3 Hz, 1H), 1.38 (d, *J* = 6.4 Hz, 3H). The remaining product aryl and Si CH_3 proton signals are obscured by residual dimethyl phenyl silane peaks at 7.52, 7.33, and 0.32 ppm. Residual Si-H peak observed at 4.43 ppm (heptet, *J* = 3.5 Hz). Mesitylene internal standard observed at 6.78 and 2.25 ppm.

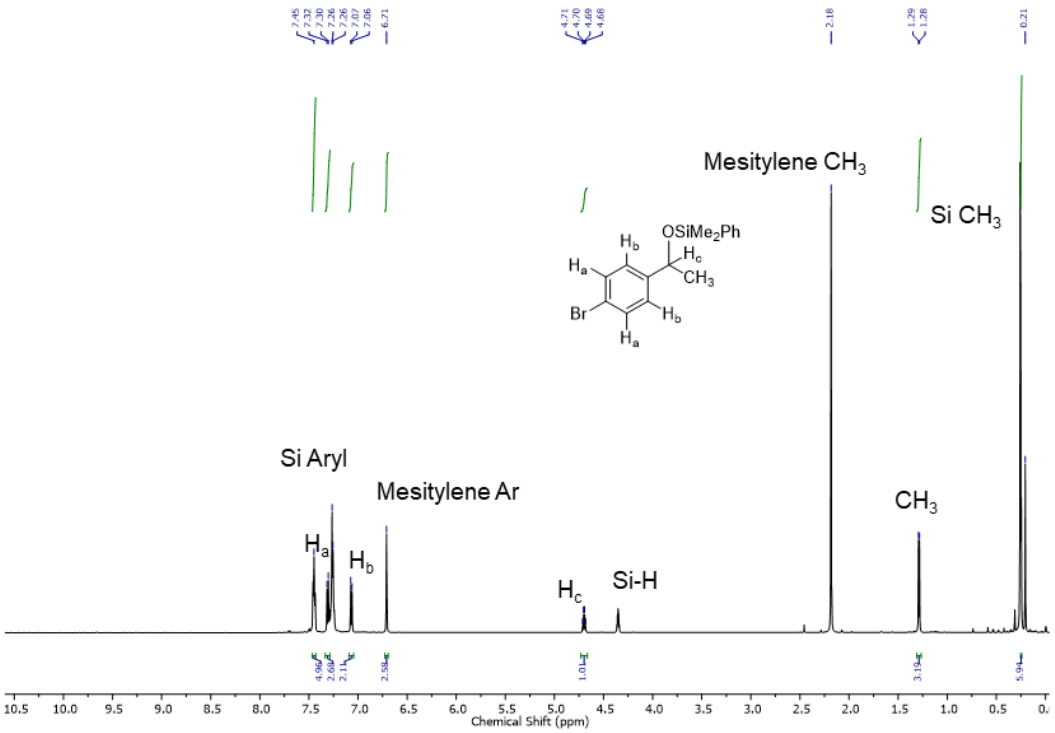

Figure S7. ^{1}H NMR Spectrum of dimethyl(phenyl)(1-(4-bromophenyl)ethoxy)silane. ^{1}H NMR (Chloroform-*d*, 600 MHz) δ: 7.39 (d, J = 8.4 Hz, 2H), 7.15 (d, J = 8.3 Hz, 2H), 4.78 (q, J = 6.3 Hz, 1H), 1.37 (d, J = 6.4 Hz, 3H), 0.33 (s, 6H). The remaining product aryl and Si CH_3 proton signals are obscured by residual dimethyl phenyl silane peaks at 7.53 and 7.34 ppm. Residual Si-H peak observed at 4.43 ppm (heptet, J = 3.5 Hz). Mesitylene internal standard observed at 6.79 and 2.26 ppm.

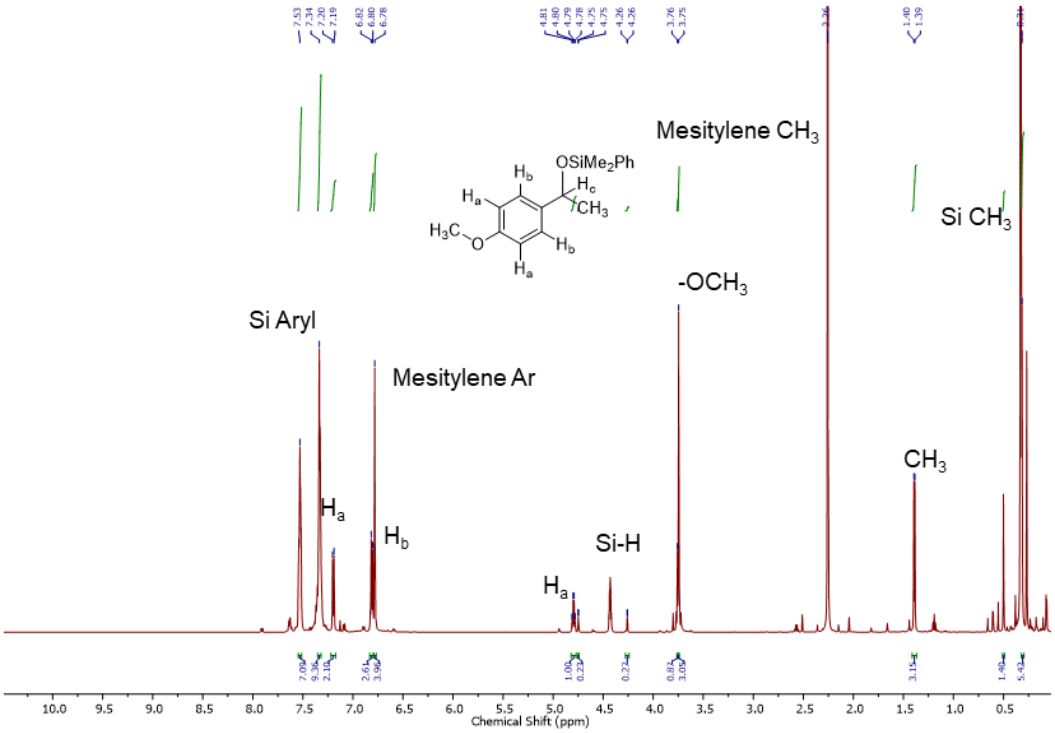

Figure S8. ^{1}H NMR Spectrum of dimethyl(phenyl)(1-(4-methoxyphenyl)ethoxy)silane. ^{1}H NMR (Chloroform-*d*, 600 MHz) δ: 7.20 (d, *J* = 8.6 Hz, 2H), 6.81 (d, *J* = 8.6 Hz, 2H), 4.80 (q, *J* = 6.3 Hz, 1H), 3.75 (s, 3H), 1.39 (d, *J* = 6.4 Hz, 3H), 0.50 (s, 1H), 0.31 (s, 6H). Peaks corresponding to the silyl enol ether are observed in a 1:4 ratio with the major product at 4.76 (d, *J* = 1.6 Hz, 1H), 4.26 (d, *J* = 1.6 Hz, 1H), 3.76 (s, 3H), 0.50 (s, 6H). The remaining product aryl and Si CH_3 proton signals are obscured by residual dimethyl phenyl silane peaks at 7.53 and 7.34 ppm. Residual Si-H peak observed at 4.43 ppm (heptet, *J* = 3.5 Hz). Mesitylene internal standard observed at 6.79 and 2.26 ppm.

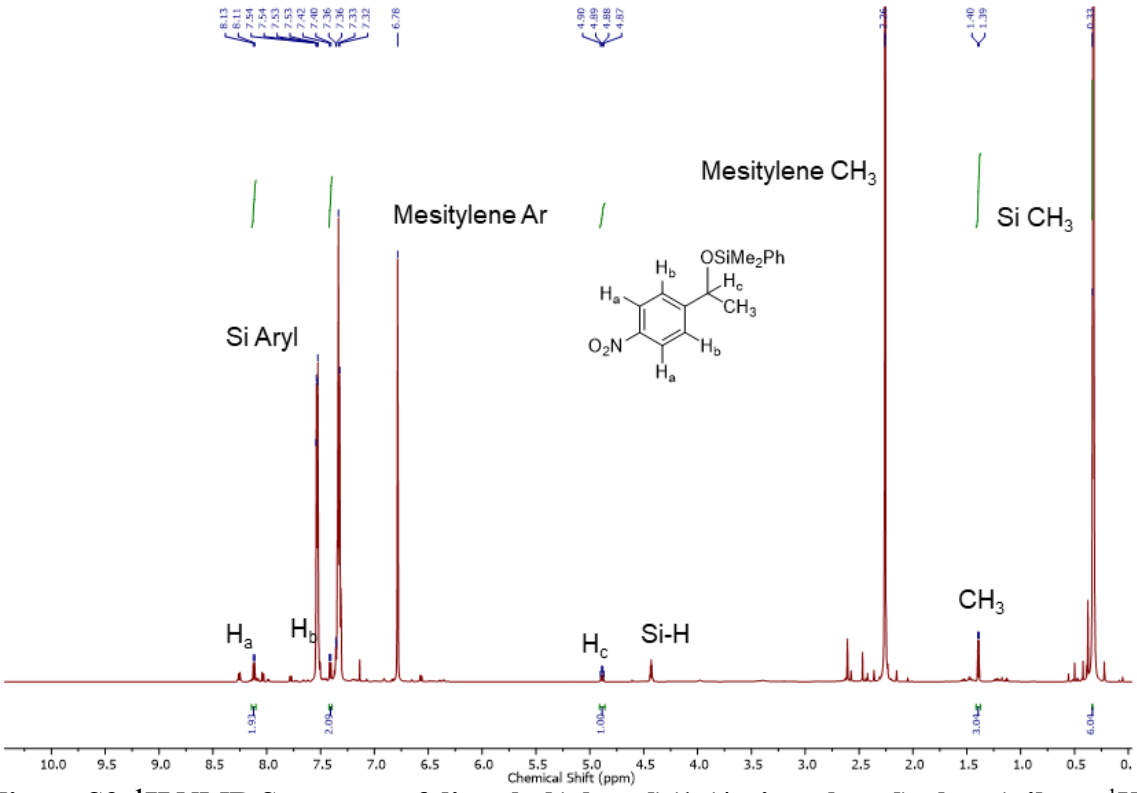

Figure S9. ^{1}H NMR Spectrum of dimethyl(phenyl)(1-(4-nitrophenyl)ethoxy)silane. ^{1}H NMR (Chloroform-*d*, 600 MHz) δ: 8.12 (d, *J* = 8.7 Hz, 2H), 7.41 (d, *J* = 8.6 Hz, 2H), 4.89 (q, *J* = 6.4 Hz, 1H), 1.39 (d, *J* = 6.4 Hz, 3H), 0.33 (s, 6H).The remaining product aryl and Si CH_3 proton signals are obscured by residual dimethyl phenyl silane peaks at 7.53 and 7.34 ppm. Residual Si-H peak observed at 4.43 ppm (heptet, *J* = 3.5 Hz). Mesitylene internal standard observed at 6.79 and 2.26 ppm.

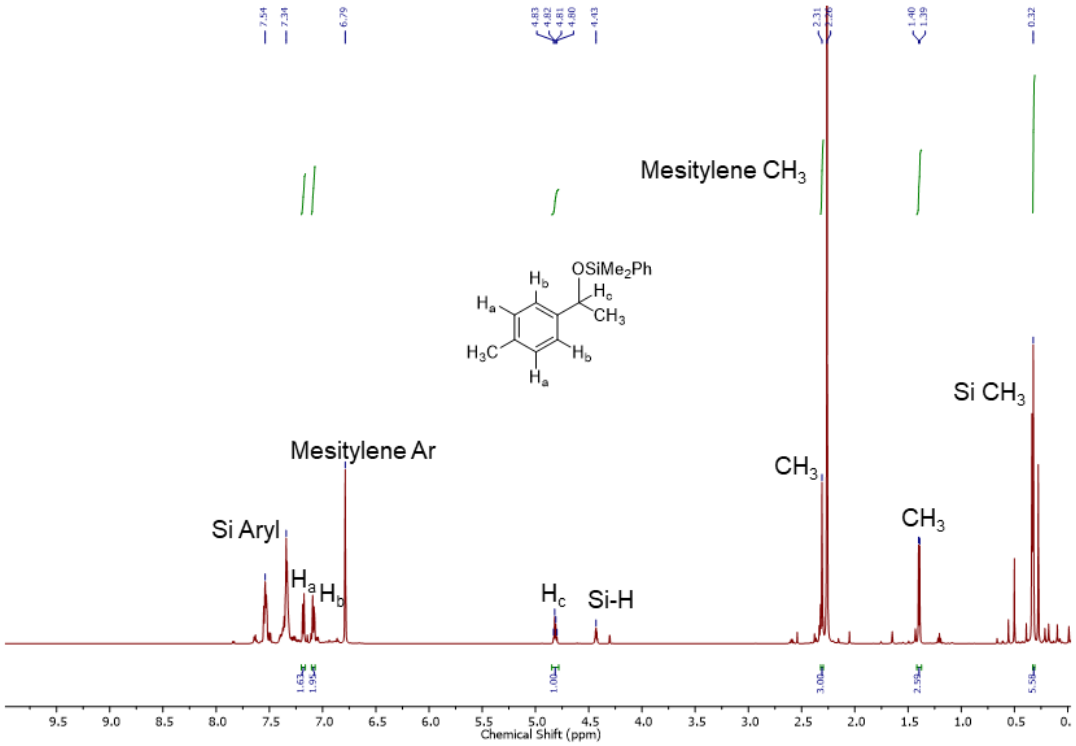

Figure S10. ^{1}H NMR Spectrum of dimethyl(phenyl)(1-*p*-tolyl)ethoxy)silane. ^{1}H NMR (Chloroform-*d*, 600 MHz) δ: 7.18 (d, *J* = 7.8 Hz, 2H), 7.10 (d, *J* = 7.8 Hz, 2H), 4.81 (q, J = 6.2 Hz, 1H), 2.31 (s, 3H), 1.40 (d, *J* = 6.4 Hz, 3H), 0.32 (s, 6H).The remaining product aryl and Si CH_3 proton signals are obscured by residual dimethyl phenyl silane peaks at 7.53 and 7.34 ppm. Residual Si-H peak observed at 4.43 ppm (heptet, *J* = 3.5 Hz). Mesitylene internal standard observed at 6.79 and 2.26 ppm.

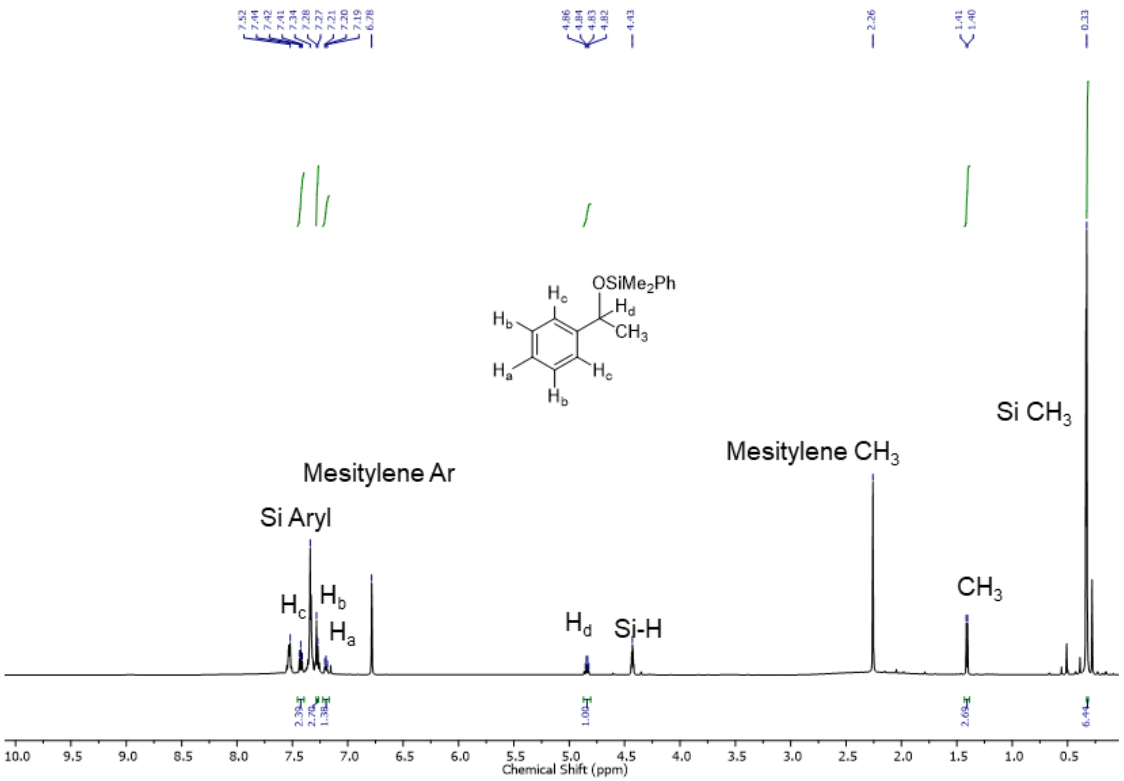

Figure S11. ^{1}H NMR Spectrum of dimethyl(phenyl)(1-phenylethoxy)silane. ^{1}H NMR (Chloroform-*d*, 600 MHz) δ: 7.42 (t, *J* = 7.7 Hz, 2H), 7.28 (d, *J* = 6.9 Hz, 3H), 7.20 (t, *J* = 6.7 Hz, 1H), 4.84 (q, *J* = 6.4 Hz, 1H), 1.41 (d, *J* = 6.4 Hz, 3H), 0.33 (s, 6H). The remaining product aryl and Si CH_3 proton signals are obscured by residual dimethyl phenyl silane peaks at 7.53 and 7.34 ppm. Residual Si-H peak observed at 4.43 ppm (heptet, *J* = 3.5 Hz). Mesitylene internal standard observed at 6.79 and 2.26 ppm.

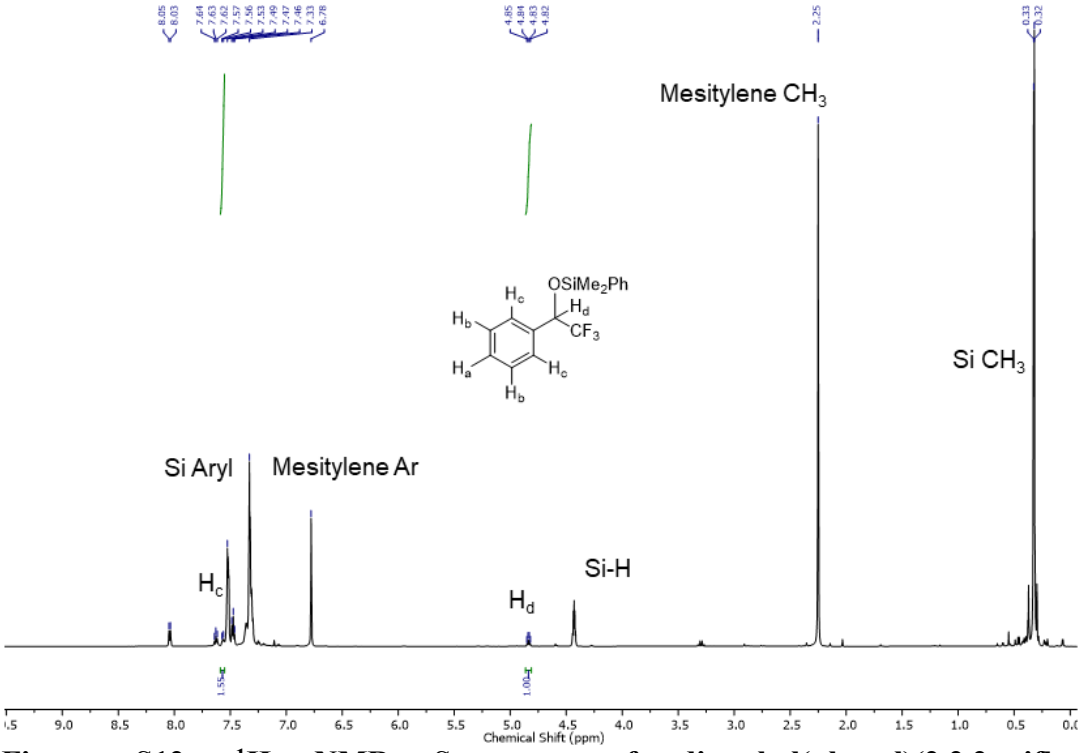

Figure S12. ^{1}H NMR Spectrum of dimethyl(phenyl)(2,2,2-trifluoro-1-phenylethoxy)silane. ^{1}H NMR (Chloroform-*d*, 600 MHz) δ: 7.57 (d, J = 7.4 Hz, 2H), 4.84 (q, J^{3} H-C-C-F = 6.6 Hz, 1H). The remaining product aryl and Si CH_3 proton signals are obscured by residual dimethyl phenyl silane peaks at 7.53 and 7.34 ppm. Residual Si-H peak observed at 4.43 ppm (heptet, J = 3.5 Hz). Mesitylene internal standard observed at 6.79 and 2.26 ppm. Unreacted starting material observed at 8.05 and 7.49 ppm.

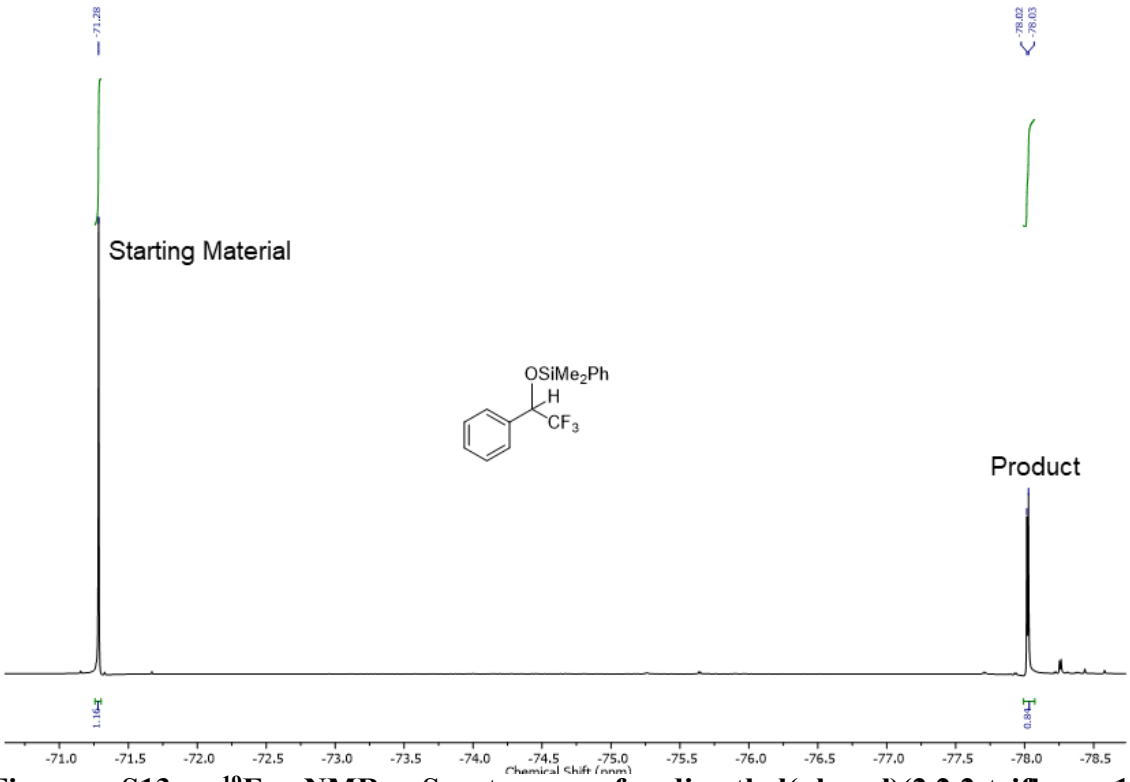

Figure S13. ^{19}F NMR Spectrum of dimethyl(phenyl)(2,2,2-trifluoro-1-phenylethoxy)silane. ^{19}F NMR (Chloroform-*d*, 564 MHz) δ: -71.28, -77.99 (d).

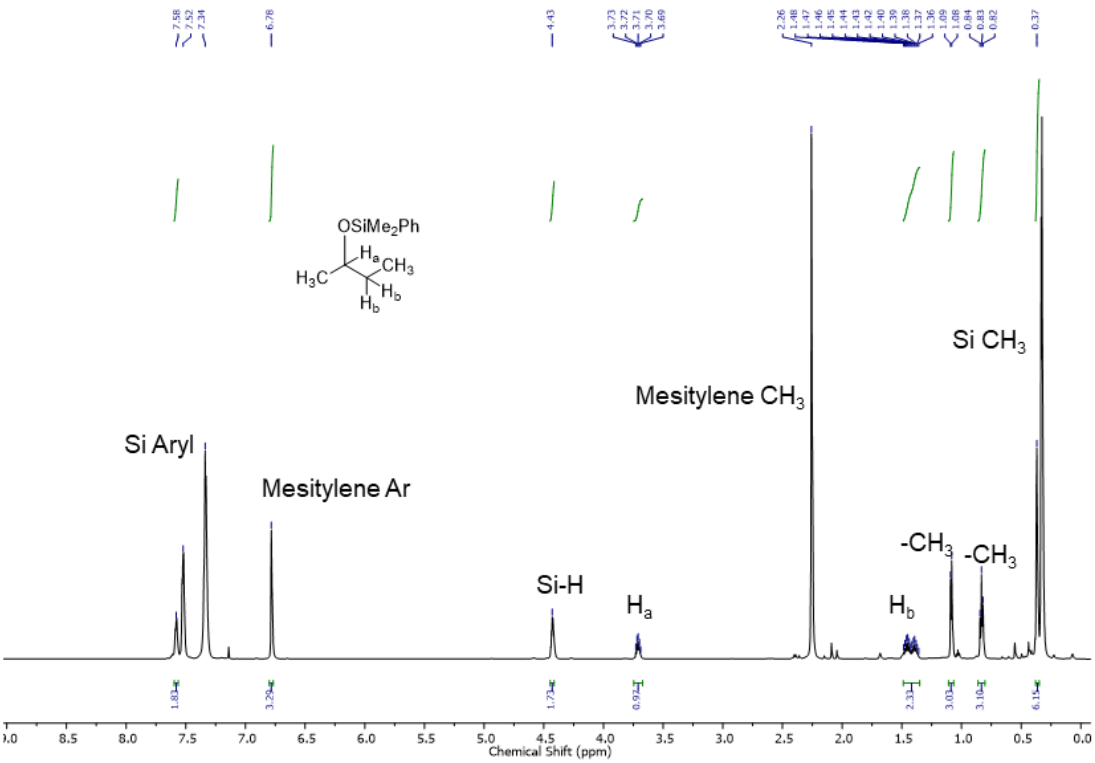

Figure S14. ^{1}H NMR Spectrum of sec-butoxydimethyl(phenyl)silane. ^{1}H NMR (Chloroform-*d*, 600 MHz) δ: 7.58 (d, *J* = 5.1 Hz, 2H), 3.71 (m, 1H), 1.42 (m, 2H), 1.09 (d, *J* = 6.1 Hz, 3H), 0.83 (t, *J* = 7.4 Hz, 3H), 0.37 (s, 6H).The remaining product aryl and Si CH_3 proton signals are obscured by residual dimethyl phenyl silane peaks at 7.53 and 7.34 ppm. Residual Si-H peak observed at 4.43 ppm (heptet, *J* = 3.5 Hz). Mesitylene internal standard observed at 6.79 and 2.26 ppm.

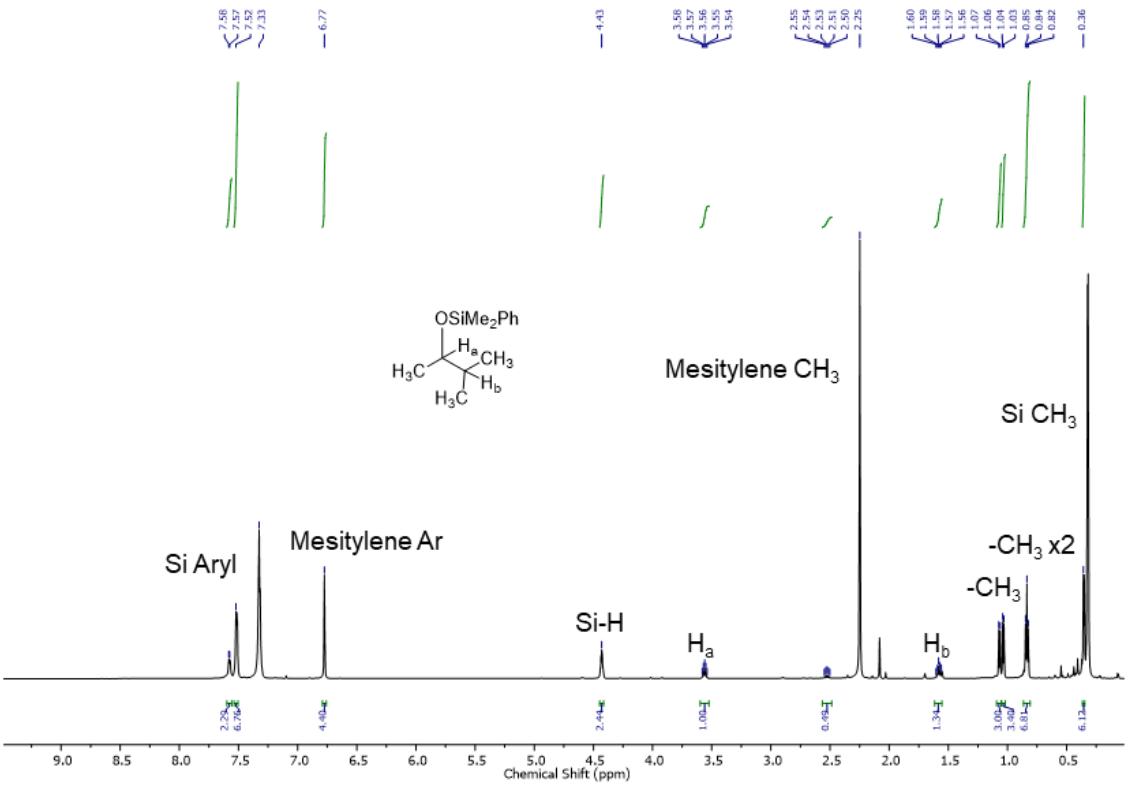

Figure S15. ^{1}H NMR Spectrum of dimethyl((3-methylbutan-2-yl)oxy)(phenyl)silane. ^{1}H NMR (Chloroform-*d*, 600 MHz) δ: 7.58 (d, *J* = 4.5 Hz, 2H), 3.56 (m, 1H), 1.62 – 1.55 (m, 1H), 1.04 (d, *J* = 6.2 Hz, 3H), 0.84 (t, *J* = 7.1 Hz, 6H), 0.36 (s, 6H).The remaining product aryl and Si CH_3 proton signals are obscured by residual dimethyl phenyl silane peaks at 7.53 and 7.34 ppm. Residual Si-H peak observed at 4.43 ppm (heptet, *J* = 3.5 Hz). Mesitylene internal standard observed at 6.79 and 2.26 ppm. Unreacted starting material observed at 2.51, 2.08, and 1.07 ppm.

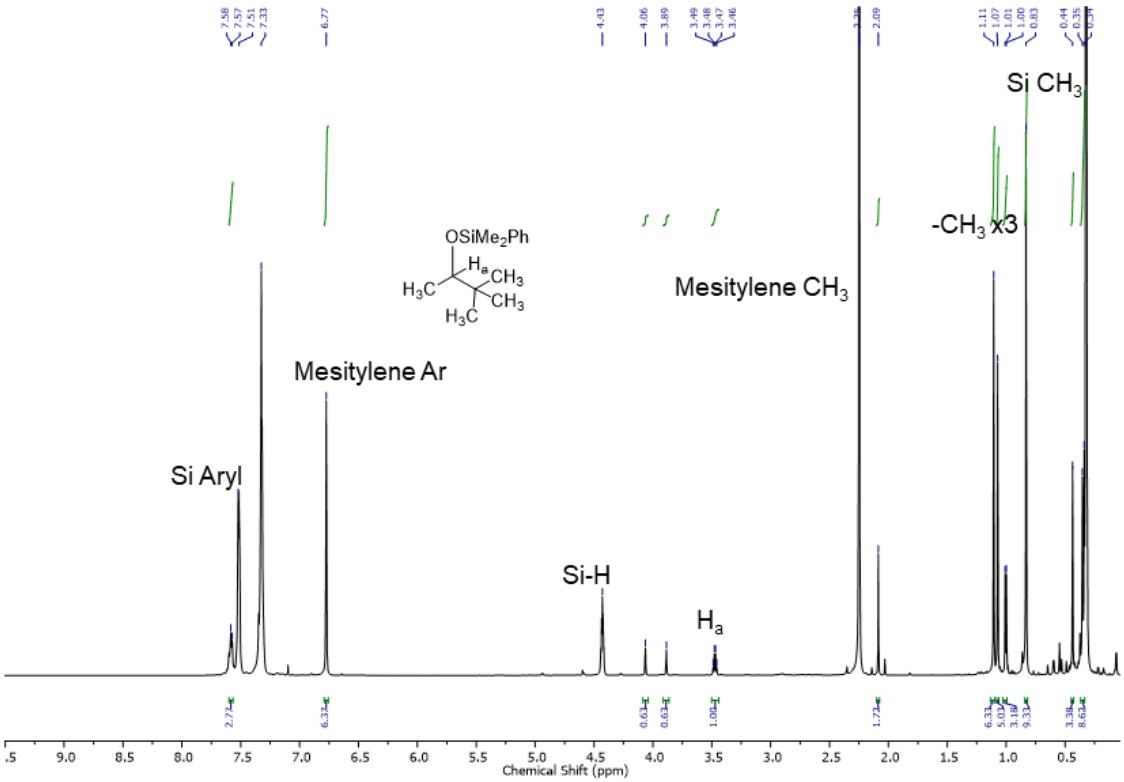

Figure S16. ^{1}H NMR Spectrum of ((3,3-dimethylbutan-2-yl)oxy)dimethyl(phenyl)silane. ^{1}H NMR (Chloroform-*d*, 600 MHz) δ: 7.58 (d, *J* = 7.5 Hz, 4H), 3.47 (q, *J* = 6.3 Hz, 1H), 1.00 (d, J = 6.3 Hz, 3H), 0.83 (s, 9H), 0.34 (s, 6H).Peaks corresponding to the silyl enol ether are observed in a 1:2 ratio with the major product at 4.06 (s, 1H), 3.89 (s, 1H), 1.11 (s, 9H), 0.44 (s, 3H). The remaining product aryl and Si CH_3 proton signals are obscured by residual dimethyl phenyl silane peaks at 7.53 and 7.34 ppm. Residual Si-H peak observed at 4.43 ppm (heptet, *J* = 3.5 Hz). Mesitylene internal standard observed at 6.79 and 2.26 ppm. Unreacted starting material observed at 2.09, and 1.07 ppm.

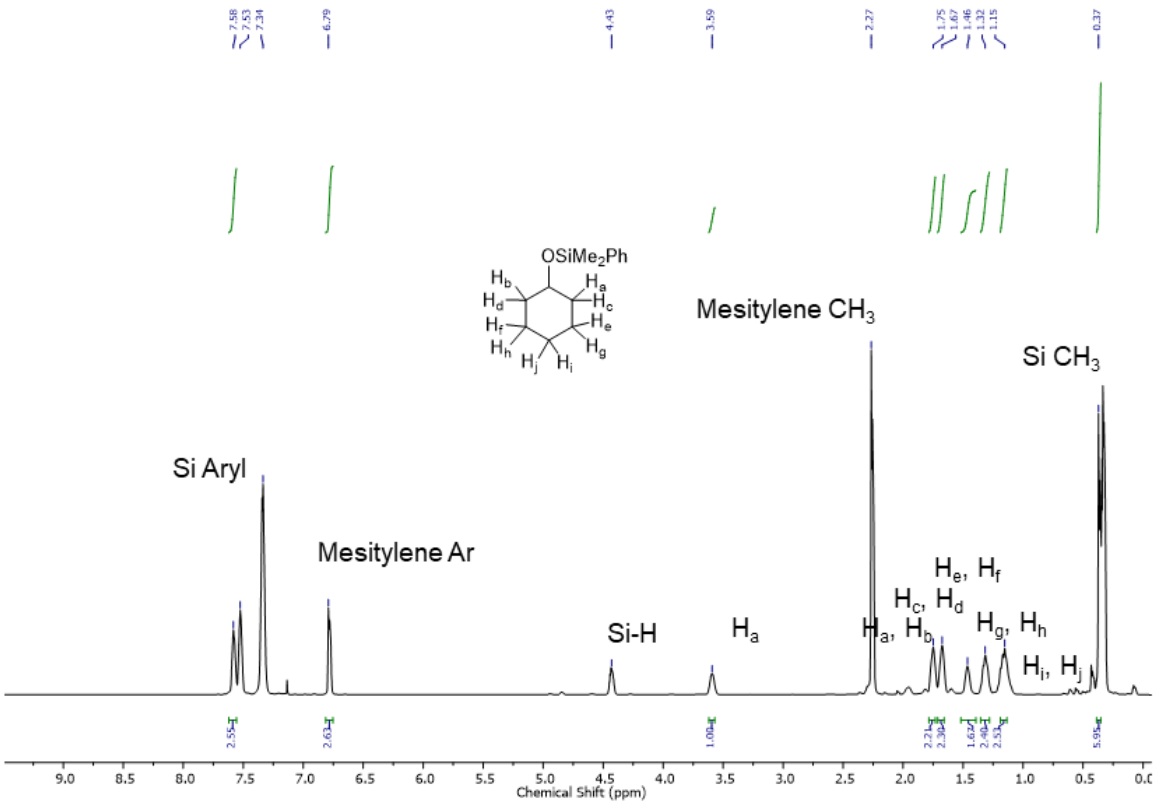

Figure S17. ^{1}H NMR Spectrum of (cyclohexyloxy)dimethyl(phenyl)silane. ^{1}H NMR (Chloroform-*d*, 600 MHz) δ: 7.58 (m, 2H), 3.59 (m, 1H), 1.75 (m, 2H), 1.67 (m, 2H), 1.46 (m, 2H), 1.32 (m, 2H), 1.15 (m, 3H), 0.37(s, 6H). The remaining product aryl and Si CH_3 proton signals are obscured by residual dimethyl phenyl silane peaks at 7.53 and 7.34 ppm. Residual Si-H peak observed at 4.43 ppm (heptet, J = 3.5 Hz). Mesitylene internal standard observed at 6.79 and 2.26 ppm.

COMPUTATIONAL DETAILS

Full Gaussian09 Citation

Gaussian 09, Revision D.01, Frisch, M. J.; Trucks, G. W.; Schlegel, H. B.; Scuseria, G. E.; Robb, M. A.; Cheeseman, J. R.; Scalmani, G.; Barone, V.; Mennucci, B.; Petersson, G. A.; Nakatsuji, H.; Caricato, M.; Li, X.; Hratchian, H. P.; Izmaylov, A. F.; Bloino, J.; Zheng, G.; Sonnenberg, J. L.; Hada, M.; Ehara, M.; Toyota, K.; Fukuda, R.; Hasegawa, J.; Ishida, M.; Nakajima, T.; Honda, Y.; Kitao, O.; Nakai, H.; Vreven, T.; Montgomery, J. A., Jr.; Peralta, J. E.; Ogliaro, F.; Bearpark, M.; Heyd, J. J.; Brothers, E.; Kudin, K. N.; Staroverov, V. N.; Kobayashi, R.; Normand, J.; Raghavachari, K.; Rendell, A.; Burant, J. C.; Iyengar, S. S.; Tomasi, J.; Cossi, M.; Rega, N.; Millam, M. J.; Klene, M.; Knox, J. E.; Cross, J. B.; Bakken, V.; Adamo, C.; Jaramillo, J.; Gomperts, R.; Stratmann, R. E.; Yazyev, O.; Austin, A. J.; Cammi, R.; Pomelli, C.; Ochterski, J. W.; Martin, R. L.; Morokuma, K.; Zakrzewski, V. G.; Voth, G. A.; Salvador, P.; Dannenberg, J. J.; Dapprich, S.; Daniels, A. D.; Farkas, Ö.; Foresman, J. B.; Ortiz, J. V.; Cioslowski, J.; Fox, D. J. Gaussian, Inc., Wallingford CT, 2009.

Computational Methods. Theoretical calculations have been carried out using the Gaussian 09[1] implementation of B3PW91[2, 3] density functional theory with the D3 version of Grimme's empirical dispersion correction.[4] All geometry optimizations were carried out in the gas phase using tight convergence criteria ("opt = tight") and pruned ultrafine grids ("Int = ultrafine"). The basis set for rhenium was the small-core (311111,22111,411) → [6s5p3d] Stuttgart-Dresden basis set and relativistic effective core potential (RECP) combination (SDD) with an additional f polarization function.[5-18] The 6-31G(d,p) basis set[19] was used for all other atoms. All structures were fully optimized. Analytical frequency calculations were performed on all structures to ensure either a zeroth-order saddle point, (a local minimum), or a first-order saddle point (transition state: TS) was achieved. The minima associated with each transition state were determined by animation of the imaginary frequency.

Energetics were calculated on the gas phase optimized structures as described above with the 6-311++G(d,p)[20] basis set for C, H, N, O, Si, B, Al, and F atoms and the SDD[5-17, 21] basis set with an added f polarization function[18] on Re. Reported energies utilized analytical frequencies and the zero point corrections from the gas phase optimized geometries.

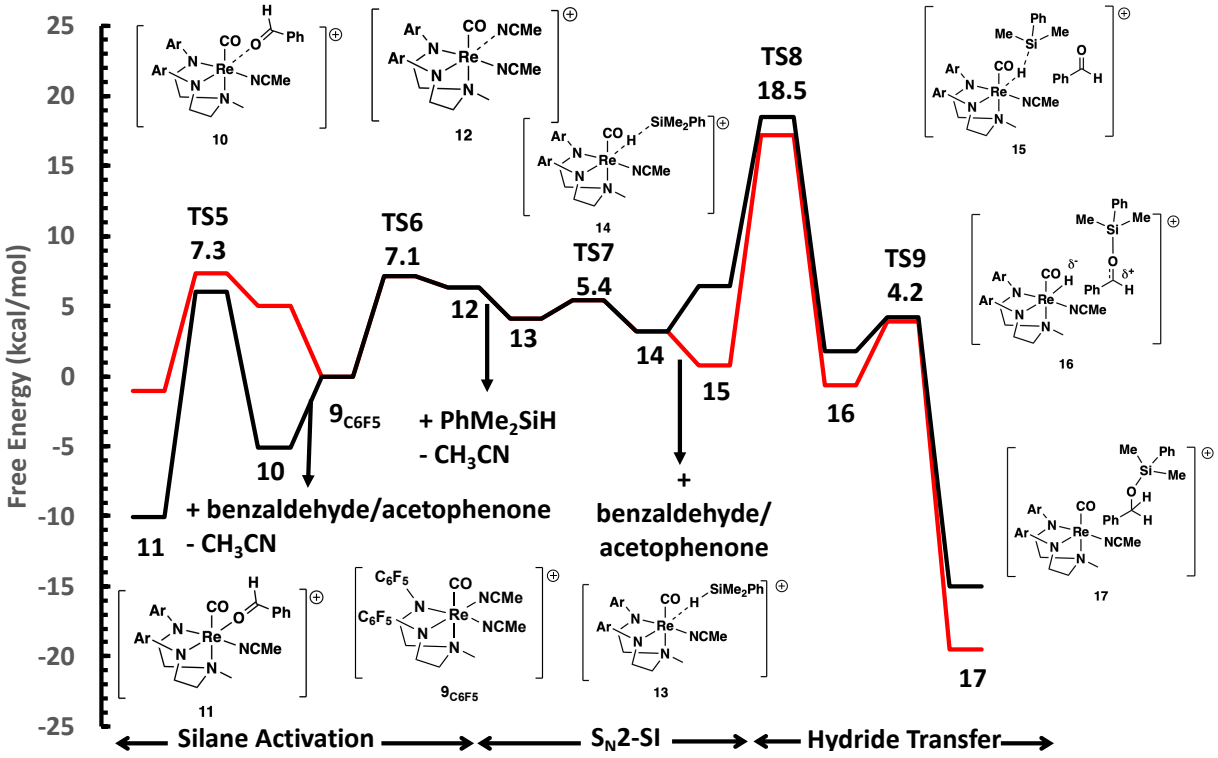

Figure S18. Comparison of pathways for the catalytic hydrosilylation of acetophenone (black) with benzaldehyde with the catalyst $[DAAmRe(CO)(NCCH_3)_2]^+$ (DAAm = *N*,*N*-bis(2-arylaminoethyl)methylamine; aryl = C_6F_5).

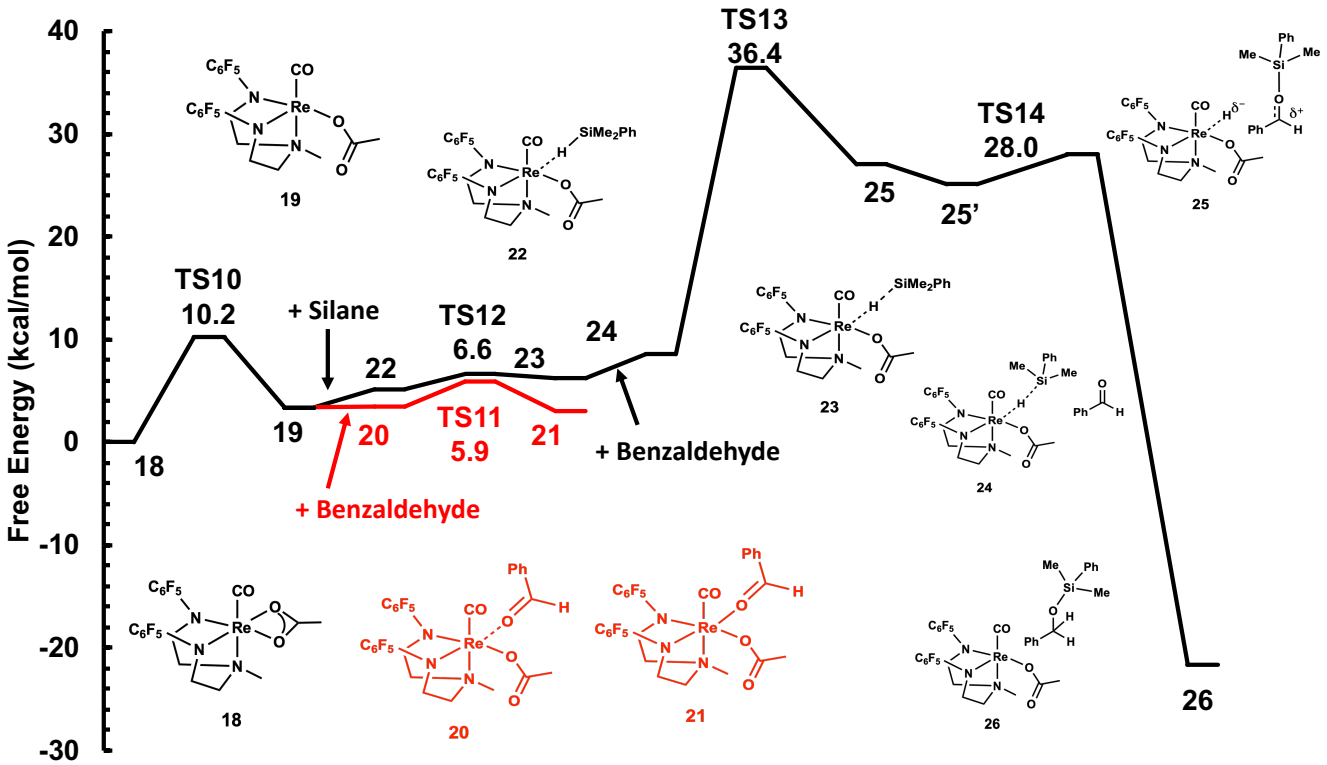

Figure S19. Calculated pathway for catalytic hydrosilylation of with benzaldehyde with the catalyst DAAmRe(CO)(OAc) (DAAm = *N*,*N*-bis(2-arylaminoethyl)methylamine; aryl = C_6F_5).

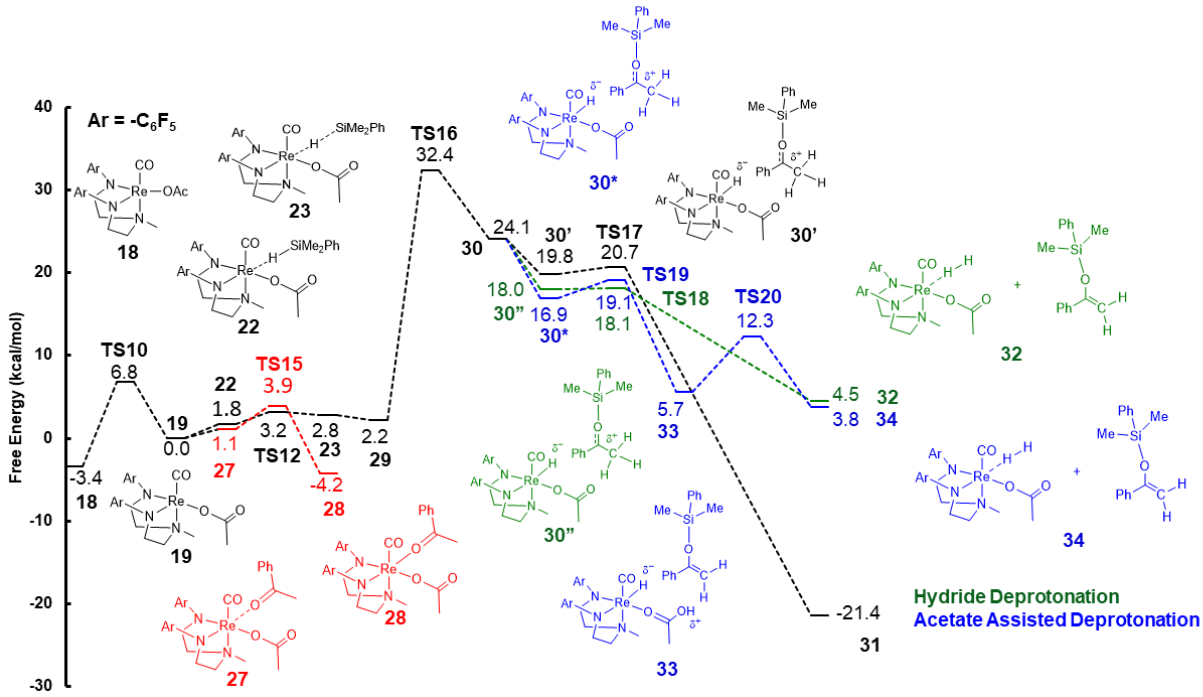

Figure S20. Calculated (B3PW91-D3) Pathway for the Formation of Silyl Enol Ether during Catalysis with **18.** See experimental section for computational details.

Summary of computational steps.

Step 1. Isomerization of **18** from κ^2 to κ^1 bound acetate **19**

Step 2. Binding of acetophenone to **19** to form **28**

Step 3. η^1 activation silane by **19** to generate the FLP **23**

Step 4. S_NSi on activated silane FLP **23** by acetophenone to produce the ion pair **30**

Step 5. Isomerization of **30** to **30'**

Step 6. Hydride transfer to release the product **31**

Alternate Step 5. Isomerization of **30** to **30''**

Alternate Step 6. Deprotonation of an α proton by the rhenium hydride to give the hydrogen bound complex **32**

Alternate Step 5. Isomerization of **30** to **30***

Alternate Step 6. Deprotonation of an α proton by the acetate ligand to give the acetic acid bound complex **33**

Alternate Step 7. Proton transfer from the bound acetic acid to the rhenium hydride to produce the hydrogen bound complex **34**

REFERENCES

1. Frisch, M.; Trucks, G.; Schlegel, H.; Scuseria, G.; Robb, M.; Cheeseman, J.; Scalmani, G.; Barone, V.; Mennucci, B.; Petersson, G., Gaussian 09. Wallingford, CT: Gaussian. Inc: 2009.
2. Becke, A. D., Density-functional exchange-energy approximation with correct asymptotic behavior. *Physical review A* **1988,** *38*, 3098.
3. Becke, A. D., Density‐functional thermochemistry. III. The role of exact exchange. *The Journal of chemical physics* **1993,** *98*, 5648-5652.
4. Grimme, S.; Antony, J.; Ehrlich, S.; Krieg, H., A consistent and accurate ab initio parametrization of density functional dispersion correction (DFT-D) for the 94 elements H-Pu. *The Journal of Chemical Physics* **2010,** *132*, 154104.
5. Cao, X.; Dolg, M., Valence basis sets for relativistic energy-consistent small-core lanthanide pseudopotentials. *The Journal of Chemical Physics* **2001,** *115*, 7348-7355.
6. Cao, X.; Dolg, M., Segmented contraction scheme for small-core lanthanide pseudopotential basis sets. *Journal of Molecular Structure: THEOCHEM* **2002,** *581*, 139-147.
7. Leininger, T.; Nicklass, A.; Stoll, H.; Dolg, M.; Schwerdtfeger, P., The accuracy of the pseudopotential approximation. II. A comparison of various core sizes for indium pseudopotentials in calculations for spectroscopic constants of InH, InF, and InCl. *The Journal of Chemical Physics* **1996,** *105*, 1052-1059.
8. Nicklass, A.; Dolg, M.; Stoll, H.; Preuss, H., Ab initio energy‐adjusted pseudopotentials for the noble gases Ne through Xe: Calculation of atomic dipole and quadrupole polarizabilities. *The Journal of Chemical Physics* **1995,** *102*, 8942-8952.
9. Küchle, W.; Dolg, M.; Stoll, H.; Preuss, H., Energy‐adjusted pseudopotentials for the actinides. Parameter sets and test calculations for thorium and thorium monoxide. *The Journal of Chemical Physics* **1994,** *100*, 7535-7542.
10. Dolg, M.; Stoll, H.; Preuss, H.; Pitzer, R. M., Relativistic and correlation effects for element 105 (hahnium, Ha): a comparative study of M and MO (M = Nb, Ta, Ha) using energy-adjusted ab initio pseudopotentials. *The Journal of Physical Chemistry* **1993,** *97*, 5852-5859.
11. Häussermann, U.; Dolg, M.; Stoll, H.; Preuss, H.; Schwerdtfeger, P.; Pitzer, R. M., Accuracy of energy-adjusted quasirelativistic ab initio pseudopotentials. *Mol. Phys.* **1993,** *78*, 1211-1224.
12. Fuentealba, P.; Szentpaly, L. v.; Preuss, H.; Stoll, H., Pseudopotential calculations for alkaline-earth atoms. *Journal of Physics B: Atomic and Molecular Physics* **1985,** *18*, 1287-1296.
13. Stoll, H.; Fuentealba, P.; Schwerdtfeger, P.; Flad, J.; Szentpály, L. v.; Preuss, H., Cu and Ag as one‐valence‐electron atoms: CI results and quadrupole corrections for Cu2, Ag2, CuH, and AgH. *The Journal of Chemical Physics* **1984,** *81*, 2732-2736.
14. Fuentealba, P.; Stoll, H.; Szentpaly, L. v.; Schwerdtfeger, P.; Preuss, H., On the reliability of semi-empirical pseudopotentials: simulation of Hartree-Fock and

Dirac-Fock results. *Journal of Physics B: Atomic and Molecular Physics* **1983,** *16*, L323-L328.
15. von Szentpály, L.; Fuentealba, P.; Preuss, H.; Stoll, H., Pseudopotential calculations on Rb+2, Cs+2, RbH+, CsH+ and the mixed alkali dimer ions. *Chem. Phys. Lett.* **1982,** *93*, 555-559.
16. Fuentealba, P.; Preuss, H.; Stoll, H.; Von Szentpály, L., A proper account of core-polarization with pseudopotentials: single valence-electron alkali compounds. *Chem. Phys. Lett.* **1982,** *89*, 418-422.
17. Dunning, T. H.; Hay, P. J., Methods of electronic structure theory. In *Modern theoretical chemistry*, Plenum Press New York: 1977; Vol. 3, p 1.
18. Ehlers, A.; Böhme, M.; Dapprich, S.; Gobbi, A.; Höllwarth, A.; Jonas, V.; Köhler, K.; Stegmann, R.; Veldkamp, A.; Frenking, G., A set of f-polarization functions for pseudo-potential basis sets of the transition metals Sc– Cu, Y‑Ag and La‑ Au. *Chem. Phys. Lett.* **1993,** *208*, 111-114.
19. Hehre, W. J.; Ditchfield, R.; Pople, J. A., Self—consistent molecular orbital methods. XII. Further extensions of Gaussian—type basis sets for use in molecular orbital studies of organic molecules. *The Journal of Chemical Physics* **1972,** *56*, 2257-2261.
20. Krishnan, R.; Binkley, J. S.; Seeger, R.; Pople, J. A., Self ‑ consistent molecular orbital methods. XX. A basis set for correlated wave functions. *The Journal of Chemical Physics* **1980,** *72*, 650-654.
21. Bergner, A.; Dolg, M.; Küchle, W.; Stoll, H.; Preuß, H., Ab initio energy-adjusted pseudopotentials for elements of groups 13–17. *Mol. Phys.* **1993,** *80*, 1431-1441.